Electrical and optical properties of a bolometer with a suspended absorber and tunneling-current thermometers

M. Tarasov,[1,2,3] V. Edelman,[2] S. Mahashabde,[4] M. Fominsky,[1] S. Lemzyakov,[2,5] A. Chekushkin,[1,5] R. Yusupov,[1,5] D. Winkler,[3] and A. Yurgens[3]
[1]*Kotelnikov Institute of Radio Engineering and Electronics RAS, Mokhovaya 11/7, 125009 Moscow, Russia*
[2]*Kapitza Institute for Physical Problems RAS, Kosygina 2, 119334 Moscow, Russia*
[3]*Chalmers University of Technology, Microtechnology and Nanoscience, Kemivagen 9, Göteborg 41296, Sweden*
[4]*Department of Physics-Astrophysics, University of Oxford, Keble Road, OX1 3RH Oxford, United Kingdom*
[5]*Moscow Institute of Physics and Technology (State University), Institutsky per. 9, 141700 Dolgoprudny, Russia*

(Received 26 April 2017; accepted 31 May 2017; published online 15 June 2017)

We have developed a bolometer with a suspended normal-metal absorber connected to superconducting leads via tunneling barriers. Such an absorber has reduced heat losses to the substrate, which greatly increases the responsivity of the bolometer to over 10^9 V/W at 75 mK when measured by dc Joule heating of the absorber. For high-frequency experiments, the bolometers have been integrated in planar twin-slot and log-periodic antennas. At 300 GHz and 100 mK, the bolometer demonstrates the voltage and current response of 3×10^8 V/W and 1.1×10^4 A/W, respectively, corresponding to the quantum efficiency of ~15 electrons per photon. An effective thermalization of electrons in the absorber favors the high quantum efficiency. We also report on how the in-plane- and transverse magnetic fields influence the device characteristics. [http://dx.doi.org/10.1063/1.4986463]

In superconducting bolometers, the electromagnetic radiation increases the temperature T_e of the electron system in a normal-metal (N) absorber. Superconducting (S) leads connected to the absorber through insulating barriers (I) form tunneling junctions. The tunneling current across such a junction is a strong function of T_e, which thereby offers a sensitive readout of the radiation power. At the low bath temperature T, the absorbed photon energy $hf \gg k_B T$ is distributed among quasiparticles through their multiple interactions and is eventually lost into the cold bath through electrical contacts and a substrate. Here, h is the Planck constant, f is the frequency of incident radiation, and k_B is the Boltzmann constant. The balance between the radiation- and cooling-powers determines T_e. Decoupling the absorber from the heat sinks would increase T_e and the detector response through the multiplication of excited electrons. It should be remembered that for the photon energy $hf \gg k_B T_e$, the energy distribution of electrons can be substantially different from the Fermi distribution, depending on the quasiparticle interactions and tunneling rate of the excited electrons through the SIN junction. For estimations of bolometric sensitivity, it is usually assumed that the absorbed radiation is equivalent to dc Joule heating of the same power.

Heat loss from an absorber can be reduced by fabricating the absorber on, e.g., a silicon nitride membrane supported by metallic thin-film beams having a small thermal conductance.[1] Also, the effective thermal capacity of absorbers fabricated on a membrane is smaller than for absorbers on a bulk substrate.[2] Further improvements can be achieved if an absorber is suspended without any supporting membrane. For an electron that absorbs a 300 GHz photon, the electron-phonon and electron-electron scattering times are about 0.2 ns and 1 ns, respectively. The excited electron creates a high-energy phonon that can easily escape from the absorber if the absorber sits on a substrate or is connected to electrodes of the same material.[3] Using different materials for the absorber and electrodes can further improve thermal insulation due to a high acoustic-impedance mismatch and increased Kapitza resistance between the absorber and electrodes. Earlier bolometers [see Fig. 1(a)] with the absorber

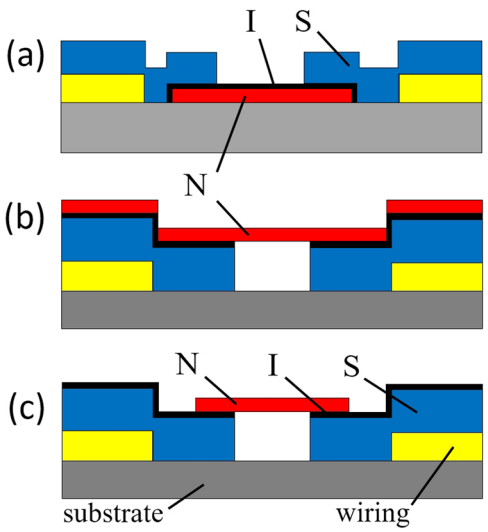

FIG. 1. Schematic views of bolometric structures. (a) Conventional SINIS-type bolometer with the absorber (N, red) lying on a substrate. (b) The bolometer with a suspended absorber that is in proximity to Au wiring and (c) the bolometer with a suspended absorber that is away from Au wiring. The absorber in (a) is oxidized to form a tunnel barrier between the absorber and the superconducting electrodes (S, blue), while in (b) and (c), it is the superconducting electrodes which are oxidized instead.

made of a non-superconducting Al thin film leak heat both into the substrate and electrodes.[4]

There have been several attempts to fabricate bolometers with suspended bridges or nano-mechanical beams. As an example, a suspended copper nanowire of $10 \times 0.3 \times 0.03$ μm^3 in size, fabricated on the Si_3N_4 membrane, demonstrated a stronger electron cooling compared to the non-suspended device.[5] Another example of a bolometer with a suspended AuPd absorber of 50 nm thickness was reported in Ref. 6. Suspended single-electron transistors fabricated with the help of reactive-ion etching of the Si substrate under 100 nm thick islands have been reported in Ref. 7. A different technique was employed in Ref. 8, where the suspended bridge was fabricated by dry etching of the underlying organic polymer in an oxygen plasma. Finally, we mention the successful chemical etching of a 100 nm thick aluminum layer under a 100 nm thick layer of Cu.[9] A bolometer composed of a Nb-AlO_x-Nb SIS tunnel junction as a thermometer thermally coupled to the suspended resistive element was realized in Ref. 10.

The above examples use relatively thick copper or gold thin films. For bolometer applications though, it is advantageous to reduce the volume of the absorber and increase its electrical resistance for better matching to the impedance of planar-antennas.

In this paper, we describe a design of a bolometer with a suspended normal-metal (N) absorber [see Figs. 1(b) and 1(c)]. The fabrication process is simpler compared to the conventional one [Fig. 1(a)] which used the shadow evaporation technique. In the design presented here, thin films can be deposited by any physical vapor deposition method including sputtering, which is difficult to use for shadow evaporation. Patterning of the normal-metal- and superconducting layers can be done by the simple lift-off process. Figure 1(b) shows a schematic view of the proposed layout. First, a trilayer of Ti (~10 nm), Au (~50 nm), and Pd (~10 nm) is deposited on the substrate. This trilayer (in yellow) is patterned for wiring and contact pads followed by the deposition of the SIN structure. Superconducting Al (~100 nm) is evaporated and oxidized in an atmosphere of pure O_2 at the pressure of 20 mbar and subsequently patterned into electrodes. Finally, the absorber normal-metal layer (20–30 nm of Pd or Cu) is deposited on the AlO_x on top of the Al electrodes. To form the suspended absorber bridge, we selectively etch the Al layer under the absorber in the region defined by a window in the resist. Aluminum under the bridge region is completely removed by etching in a weak base (Microposit™ MF CD-26 developer). The results of etching are clearly visible in the scanning electron microscope (see Fig. 2).

The first attempt to fabricate suspended absorbers used Cu thin films. However, such thin films were soft and had a tendency to sag down to the substrate. Additionally, Cu absorbers had too low resistance even for the thicknesses down to 20 nm. This prevented such devices from being impedance matched with quasi-optical antennas having impedances ~50 Ω. A thin (~3 nm) layer of Cr was added to the Cu thin-film absorber (~20 nm) to create sufficiently rigid suspended bridges. This combination of materials was found to give satisfactory results although the processing required several photolithography steps involving the delicate critical-point drying to avoid collapse of the already formed bridges. Furthermore, to investigate the proximity effect of the normal-metal wiring on the superconducting properties of the SIN junctions, an extra step of chemical etching of Cu in diluted 1:50 HNO_3 was added to the fabrication sequence to increase the distance between the wiring and junctions [see Fig. 1(c)].

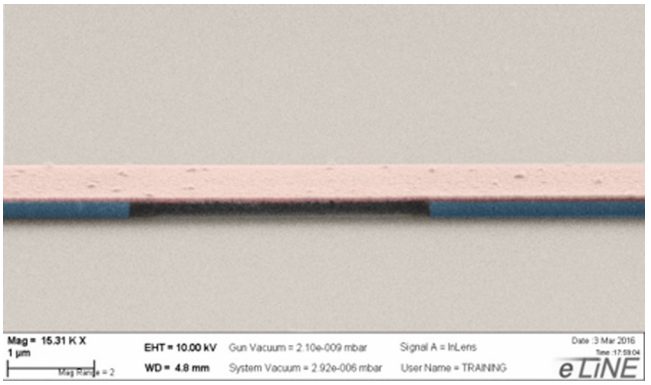

FIG. 2. SEM image of the bolometer with the suspended absorber corresponding to the schematic cross-section shown in Fig. 1(b). The suspended absorber is 3 μm long, 0.5 μm wide, and 0.023 μm thick.

The dynamic resistance of the sample with the Cu absorber and the geometry shown in Fig. 1(b) was measured at 130–480 mK. For this sample, the combined superconducting energy gap of the two SIN junctions was ~250 μeV. Adding the in-plane separation between the normal-metal wiring and the SIN junctions of 0.5 μm and 2 μm increased the energy gap to 350 μeV and 380 μeV, respectively [see Fig. 1(c)].

For clarifying the role of experimental conditions in the performance margins of the bolometer, we also measured the current-voltage (IV) characteristics and dynamic conductance in the transverse and in-plane external magnetic field. The dynamic conductance had a clear zero-bias peak (see Fig. 5). Similar results for SINIS structures were observed in Ref. 11.

A 4-probe structure was used to measure the electrical response of the bolometer by applying Joule heating across outer contacts and measuring IV curve and response for the middle contacts with single suspended bridge. The response of the bolometer for dc heating at 75 mK bath temperature corresponds to an electrical responsivity of $dV/dP > 10^9$ V/W.

Next, samples with suspended Hafnium absorbers having lower electron-phonon interaction constant were fabricated. With these bolometers integrated in a twin-slot antenna[12] and placed on an extended hemisphere sapphire lens, we measured the optical response to radiation at 300 GHz. Radiation from the black body source was filtered by band-pass- and neutral-density filters. The results are presented in Fig. 3.

The current response can be a good indicator of the quantum efficiency η of the bolometer, i.e., the number of tunneling electrons n_e induced by a single photon of radiation. For conventional cold-electron bolometers,[3,12] $\eta = 1.2$–1.5 instead of the expected $\eta = hf/k_BT = 50$ at $f = 350$ GHz, predicted by the theory for bolometric response.[13] In the case of our suspended bolometer, with the current response as in Fig. 3 (right axis) of 0.7 nA at the incident power of 0.06 pW, the current

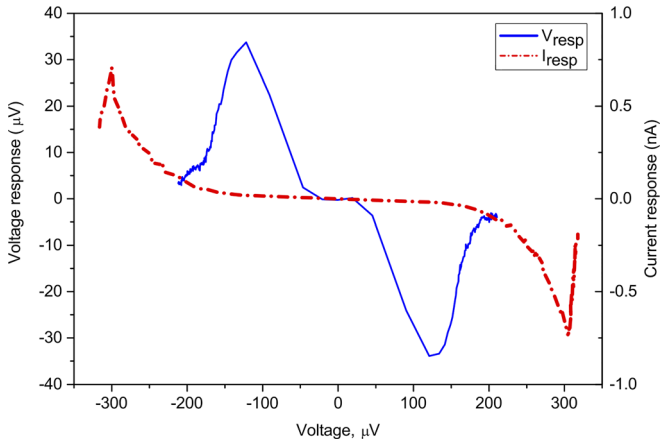

FIG. 3. Left axis: voltage response approaching 3×10^8 V/W (blue, solid line) for the sample with the Hf absorber. Right axis: current response of the sample with the Cu absorber approaching 1.1×10^4 A/W (red, dashed-dotted line).

responsivity is 1.1×10^4 A/W. As a result, a quantum gain of over 15 electrons per photon was estimated, approaching the values predicted in Ref. 13. This is a direct proof of the initial design idea to disconnect the absorber from direct contact with the substrate for improving the thermal insulation and increasing the bolometer response.

Another important feature of the suspended bolometer is the similarity in the shapes of dynamic resistance to thermal and optical heating (see Fig. 4). This indicates that in such bolometers, we can obtain an effective thermalization of the hot electrons heated by the absorbed radiation, which in turn provides a better quantum efficiency. In contrast, conventional bolometers with absorbers on substrates show a non-thermal optical response, which is a result of the non-equilibrium effects and non-Fermi energy distribution of electrons.[14]

In the conventional Blonder-Tinkham-Klapwijk theory for a NIS tunnel junction with an insulator of low transparency, the Andreev reflection is predicted to be vanishingly small. Taking into account the quasiparticle confinement in the vicinity of the interface, Andreev reflection can however increase. Such confinement can be induced by the disorder and the presence of a second barrier in the normal metal. A single quasiparticle then experiences several collisions with the interface.[15] The final

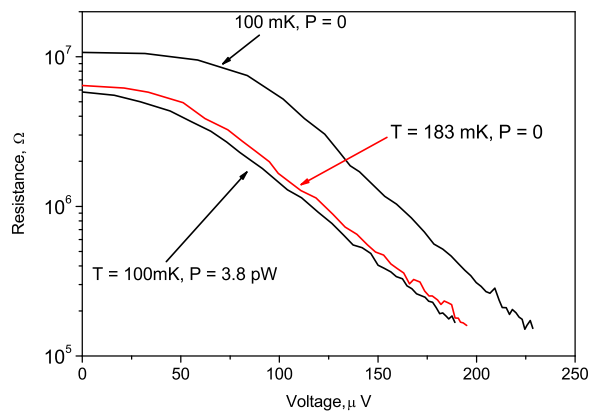

FIG. 4. The dynamic resistance of our bolometer without radiation at the bath temperatures of 100 mK and 183 mK and with 3.8 pW optical power load at 100 mK.

transmission coefficient corresponds to the addition of many individual transmission probabilities. Therefore, the subgap current significantly increases and can be altered by the in-plane magnetic field. Andreev current components can be described analytically.[15] Our measurements can be fitted by this model; for details, see Refs. 16 and 17.

Conductivity behavior dramatically changed in the transverse magnetic field [see Fig. 5(b)]. Here, conductivity increased [contrary to Fig. 5(a)]. The conductivity at zero bias voltage increased with the field by 2–4 orders of magnitude.[18] Pure bulk aluminum is a classical type-I superconductor. However, the thin films usually have a fine grain structure. In addition, aluminum can be contaminated considerably during deposition owing to its high chemical activity. As a result, the films may become a type-II superconductor, and a mixed state with Abrikosov vortices will be formed in the transverse magnetic field.

Another important issue of the SINIS bolometer and electron cooler development is a proper cooling of the superconducting electrode. The simplest way is to increase the thickness and area of the superconducting electrode, which helps to spread the injected electrons in a larger volume, thereby decreasing the local hot quasiparticles density. This is important since quasiparticle lifetimes in a superconductor like Al can be of the order of μs. Another known method is the use of a normal metal trap. One of the pioneering experimental works investigated the cooling of the 18-nm thick Al wire covered by the 28-nm thick Cu thin film deposited over the Al oxide.[19] An improvement was observed after reducing the distance from the tunnel junction to the Cu film from 8 μm to 0.2 μm.

An alternative option involved using a direct contact to a normal-metal trap resulting in the measured trapping efficiency (the ratio of absorbed to incident power), of about 10% near 100 mK.[20] In an earlier paper, the normal-metal traps were made of Au film of 60 nm thickness, with the Al superconducting electrodes of 65 nm thickness on top of it.[21] In reality, the contact between Au and Al is an intermetallic compound with high electrical resistivity. Such a contact can be viewed as a tunnel junction, even though with a relatively high transparency.[19] In the cases shown in Figs. 1(a) and 1(b), we have the Ti/Au/Pd trilayer where the top Pd makes

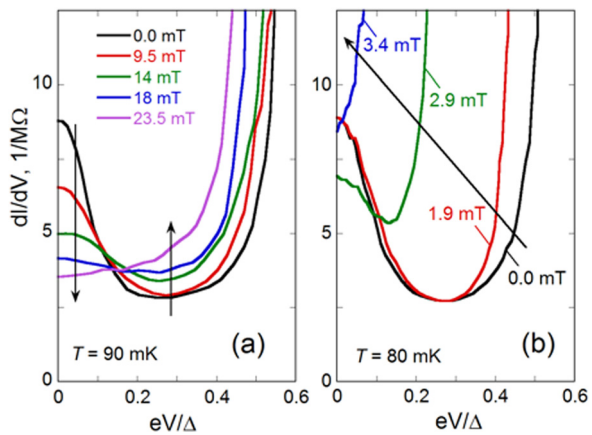

FIG. 5. The conductivity dI/dV of the SIN junction as a function of the voltage normalized to the superconducting energy gap parameter Δ for the in-plane (a) and perpendicular (b) magnetic field. The arrows indicate changes with increasing magnetic field.

the perfect contact to Al. As a result, we have a suppression of superconductivity in Al and no strong evidence of electron cooling. When introducing a separation of 1–2 μm as in Fig. 1(c), we observe the nominal value of the superconducting energy gap of Al ($\sim$380 μV).

The obtained optical responsivity of 3×10^8 V/W and actual voltage noise of 30 nV/Hz$^{1/2}$ correspond to noise equivalent power $\mathrm{NEP_V} = 10^{-16}$ W/Hz$^{1/2}$. A current responsivity of 1.1×10^4 A/W and a shot noise 0.1 pA/Hz$^{1/2}$ correspond to intrinsic $\mathrm{NEP_I} = 10^{-17}$ W/Hz$^{1/2}$. The photon noise level for the signal power of 1 pW is $\mathrm{NEP_{PHOT}} = (2P\,\mathrm{h}f)^{0.5} = 2 \times 10^{-17}$ W/Hz$^{1/2}$. Thermal fluctuations, also known as phonon noise, can be calculated as $\mathrm{NEP_{PHONON}} = (4kT^2G)^{0.5} = (10k\Sigma\nu T^6)^{0.5} = 10^{-19}$ W/Hz$^{1/2}$ that is much below other components. Spectral characteristics of our bolometers are determined by the twin-slot antenna type, as in Refs. 2 and 12 with design frequency around 300 GHz, or in the case of log-periodic antenna, it can be extended over several Terahertz. The detectivity D that is NEP normalized per square root of the sensor's area A and frequency bandwidth df is given by $D = (A\ \delta f)^{0.5}/\mathrm{NEP} = 0.75 \times 10^{18}$ (m Hz)/W and this parameter is not very informative for planar single-mode antennas with an effective area about a half wavelength square.

This work was done with support from The Swedish Foundation for International Cooperation in Research and Higher Education (STINT, Grant No. IG2010-14) and the Swedish Research Council (VR, Grant No. 621-2014-5468). The clean-room processing has been done in the Nanofabrication Laboratory on the equipment sponsored by the Knut and Alice Wallenberg Foundation.

[1]J. Gildemeister, A. Lee, and P. Richards, Appl. Phys. Lett. **74**(6), 868 (1999).
[2]L. Kuzmin, D. Chouvaev, M. Tarasov, P. Sundquist, M. Willander, and T. Claeson, IEEE Trans. Appl. Supercond. **9**(2), 3186 (1999).
[3]M. Tarasov, V. Edelman, A. Ermakov, S. Mahashabde, and L. Kuzmin, IEEE Trans. Terahertz Sci. Technol. **5**(1), 44 (2015).
[4]M. Tarasov, L. Kuzmin, and N. Kaurova, Instrum. Exp. Tech. **52**(6), 877 (2009).
[5]P. Koppinen and I. Maasilta, Phys. Rev. Lett. **102**, 165502 (2009).
[6]J. Muhonen, A. Niskanen, M. Meschke, Yu. Pashkin, J. S. Tsai, L. Sainiemi, S. Franssila, and J. Pekola, Appl. Phys. Lett. **94**, 073101 (2009).
[7]G. Paraonau and A. Halvari, Appl. Phys. Lett. **86**, 093101 (2005).
[8]T. Li, Yu. Pashkin, O. Astafiev, Y. Nakamura, J. Tsai, and H. Im, Appl. Phys. Lett. **91**, 033107 (2007).
[9]H. Nguyen, L. Pascal, Z. Peng, O. Buisson, B. Gilles, and C. Winkelmann, Appl. Phys. Lett. **100**, 252602 (2012).
[10]A. Timofeev, P. Helisto, L. Gronberg, A. Luukanen, H. Seppa, and J. Hassel, Open Appl. Phys. J. **5**, 34 (2012).
[11]S. Rajauria, P. Gandit, T. Fournier, F. W. Hekking, B. Pannetier, and H. Courtois, Phys. Rev. Lett. **100**, 207002 (2008).
[12]M. Tarasov, V. S. Edelman, S. Mahashabde, and L. Kuzmin, IEEE Trans. Appl. Supercond. **24**(6), 2400105 (2014).
[13]I. A. Devyatov and M. Yu. Kupriyanov, JETP Lett. **80**(10), 646 (2004).
[14]M. Tarasov, V. Edelman, S. Mahashabde, and L. Kuzmin, J. Exp. Theor. Phys. **119**(1), 107 (2014).
[15]F. W. J. Hekking and Yu. V. Nazarov, Phys. Rev. B **49**, 6847 (1994).
[16]A. V. Seliverstov, M. A. Tarasov, and V. S. Edel'man, JETP Lett. **103**(7), 484 (2016).
[17]A. V. Seliverstov, M. A. Tarasov, and V. S. Edelman, J. Exp. Theor. Phys. **124**(4), 643–656 (2017).
[18]M. Tarasov and V. Edelman, JETP Lett. **101**(11), 740 (2015).
[19]J. Pekola, D. Anghel, and T. Suppula, Appl. Phys. Lett. **76**(19), 2782 (2000).
[20]J. Ullom, P. Fisher, and M. Nahum, Nucl. Instrum. Methods Phys. Res., Sect. A **370**, 98 (1996).
[21]L. Kuzmin, I. Agulo, M. Fominsky, A. Savin, and M. Tarasov, Supercond. Sci. Technol. **17**, S400–S405 (2004).